



<b>Publication Year</b>	2015
<b>Acceptance in OA @INAF</b>	2020-04-15T08:52:47Z
<b>Title</b>	Radial Velocities from VLT-KMOS Spectra of Giant Stars in the Globular Cluster NGC 6388
<b>Authors</b>	Lapenna, E.; ORIGLIA, Livia; Mucciarelli, A.; Lanzoni, B.; Ferraro, F. R.; et al.
<b>DOI</b>	10.1088/0004-637X/798/1/23
<b>Handle</b>	<a href="http://hdl.handle.net/20.500.12386/24032">http://hdl.handle.net/20.500.12386/24032</a>
<b>Journal</b>	THE ASTROPHYSICAL JOURNAL
<b>Number</b>	798

## RADIAL VELOCITIES FROM VLT-KMOS SPECTRA OF GIANT STARS IN THE GLOBULAR CLUSTER NGC 6388\*

E. LAPENNA<sup>1</sup>, L. ORIGLIA<sup>2</sup>, A. MUCCIARELLI<sup>1</sup>, B. LANZONI<sup>1</sup>, F. R. FERRARO<sup>1</sup>,  
E. DALESSANDRO<sup>1</sup>, E. VALENTI<sup>3</sup>, AND M. CIRASUOLO<sup>4</sup>

<sup>1</sup> Dipartimento di Fisica e Astronomia, Università degli Studi di Bologna, Viale Berti Pichat 6/2, I-40127 Bologna, Italy

<sup>2</sup> INAF-Osservatorio Astronomico di Bologna, Via Ranzani, 1, I-40127 Bologna, Italy

<sup>3</sup> European Southern Observatory, Karl-Schwarzschild-Strasse 2, D-85748 Garching bei München, Germany

<sup>4</sup> Institute for Astronomy, University of Edinburgh & STFC, UK Astronomy Technology Center Royal Observatory, Blackford Hill, EH9 3HJ, Edinburgh, UK

Received 2014 July 17; accepted 2014 October 21; published 2014 December 15

### ABSTRACT

We present new radial velocity measurements for 82 stars, members of the Galactic globular cluster (GC) NGC 6388, obtained from ESO-VLT *K*-band Multi Object Spectrograph (KMOS) spectra acquired during the instrument Science Verification. The accuracy of the wavelength calibration and a number of tests of the KMOS response are presented. The cluster systemic velocity obtained ( $81.3 \pm 1.5 \text{ km s}^{-1}$ ) is in very good agreement with previous determinations. While a hint of ordered rotation is found between  $9''$  and  $20''$  from the cluster center, where the distribution of radial velocities is clearly bimodal, more data are needed before drawing any firm conclusions. The acquired sample of radial velocities has also been used to determine the cluster velocity dispersion (VD) profile between  $\sim 9''$  and  $70''$ , supplementing previous measurements at  $r < 2''$  and  $r > 60''$  obtained with ESO-SINFONI and ESO-FLAMES spectroscopy, respectively. The new portion of the VD profile nicely matches the previous ones, better defining the knee of the distribution. The present work clearly shows the effectiveness of a deployable integral field unit in measuring the radial velocities of individual stars for determining the VD profile of Galactic GCs. It represents the pilot project for an ongoing large program with KMOS and FLAMES at the ESO-VLT, aimed at determining the next generation of VD and rotation profiles for a representative sample of GCs.

*Key words:* globular clusters: individual (NGC 6388) – instrumentation: spectrographs – stars: kinematics and dynamics – techniques: spectroscopic

### 1. INTRODUCTION

Galactic globular clusters (GCs) are massive ( $10^4$ – $10^6 M_{\odot}$ ) stellar aggregates, where the two-body relaxation timescale is shorter than the age (e.g., Binney & Tremaine 1987). For this reason, they have been traditionally assumed to be quasi-relaxed, nonrotating systems, characterized by spherical symmetry and orbital isotropy. Hence spherical, isotropic, and non-rotating models, with a truncated distribution function close to a Maxwellian (King 1966; Wilson 1975) are commonly used to fit the observed surface brightness or density profiles, and to estimate the main GC structural parameters, like the core and half-mass radii, the concentration parameter and even the total mass, (e.g., Harris 1996; McLaughlin & van der Marel 2005).

However, recent theoretical results indicate that these systems may have not attained complete energy equipartition (Trenti & van der Marel 2013) and, depending on the degree of dynamical evolution suffered and the effect of an external tidal field, they may still preserve some characteristic kinematical feature (Vesperini et al. 2014). In particular, nonzero angular momentum has been recognized to affect the entire dynamical evolution of star clusters (Einsel & Spurzem 1999), and central rotation might still be present in GCs hosting an intermediate mass ( $10^2$ – $10^4 M_{\odot}$ ) black hole (IMBH; Fiestas & Spurzem 2010). Moreover, it is well known that the density profile alone is not sufficient to fully characterize a gravitational system, and the information about internal dynamics is also necessary (e.g., Binney & Tremaine 1987; Meylan & Heggie 1997 and references therein).

For instance, a star density profile with a shallow cusp deviating from a King (1966) model and a velocity dispersion (VD) profile with a Keplerian central behavior are predicted in the presence of an IMBH (e.g., Baumgardt et al. 2005; Miocchi 2007). Despite its importance, the kinematical properties of Galactic GCs are still poorly explored from the observational point of view, although the number of dedicated studies aimed at building their VD and rotation profiles has significantly increased in the last years (see, e.g., Anderson & van der Marel 2010; Noyola et al. 2010; Lane et al. 2010; Bellazzini et al. 2012; McNamara et al. 2012; Lützgendorf et al. 2013; Fabricius et al. 2014; Kacharov et al. 2014 and references therein). In this context, interesting insights on specific dynamical processes occurring in the central regions of some clusters have been obtained by using “exotic” stellar populations, like millisecond pulsars and blue straggler stars (see Ferraro et al. 2003, 2009, 2012). However, proper VD and rotation profiles, especially in their innermost regions where the presence of the long-searched IMBHs is expected to leave characteristic signatures (as a VD cusp and systemic rotation; Baumgardt et al. 2005; Miocchi 2007; Einsel & Spurzem 1999), are still badly constrained. This is due to the observational difficulties affecting both proper motion studies and the investigations of the velocity line-of-sight component.

As for the latter, while determining the line-of-sight rotation curve and VD profile in external galaxies is relatively simple (requiring the measurement, respectively, of the Doppler shift and the broadening of spectral lines in integrated-light spectra), it is much less straightforward in resolved stellar populations as Galactic GCs. In these systems, in fact, the dominant contribution of a few bright stars may artificially broaden the spectral lines, making the resulting value a nonrepresentative

\* Based on observations collected at the ESO-VLT (Cerro Paranal, Chile) under program 60.A-9448(A).

measure of the true VD of the underlying stellar population (this is commonly referred as “shot noise bias”; e.g., Dubath et al. 1997; Noyola et al. 2010; Lützgendorf et al. 2011). The alternative approach is to measure the dispersion about the mean of the radial velocities of statistically significant samples of individual stars. Clearly, this methodology is not prone to the shot-noise bias, provided that the individual stars are well resolved, sufficiently isolated and bright enough to be negligibly contaminated by the unresolved stellar background.

The latter approach is becoming increasingly feasible thanks to the current generation of adaptive-optics (AO) assisted spectrograph with an integral field unit (IFU), and the improved data analysis techniques (e.g., Lanzoni et al. 2013, hereafter L13; Kamann et al. 2013), as clearly demonstrated by the case of NGC 6388. The VD profile of this cluster derived from the line broadening of integrated-light spectra shows a steep cusp with a central value of 23–25 km s<sup>-1</sup>, which is best fitted by assuming that an IMBH of  $2 \times 10^4 M_{\odot}$  is hidden in the system (Lützgendorf et al. 2011). Instead, if the radial velocities of individual stars are used, a completely different result is found. By using SINFONI, an AO-assisted IFU spectrograph at the ESO-VLT, L13 measured the radial velocity of 52 individual stars in the innermost 2'' of the cluster, finding a flat VD profile with a central value of only 13–14 km s<sup>-1</sup>, which is well reproduced by no IMBH or, at most, a BH of  $\sim 2000 M_{\odot}$  (L13; see also Lanzoni et al. 2007). As discussed in detail in L13 (see their Section 4.1 and their Figure 12), the integrated light spectra measured in the innermost part of the cluster are dominated by the contribution of two bright stars having opposite radial velocities with respect to the systemic one, despite the explicit effort by Lützgendorf et al. (2011) to correct for this. This produces a spuriously large line broadening and a consequent overestimate of the central VD value.

The results obtained in NGC 6388 clearly demonstrate the feasibility of the individual radial velocity diagnostics and show that this is indeed the safest way to measure the stellar VD in Galactic GCs. To identify other multi-object facilities suitable for this kind of approach, we took advantage of the new *K*-band Multi Object Spectrograph (KMOS; Sharples et al. 2010), recently commissioned at the ESO-VLT. During the instrument Science Verification (SV) run, under proposal 60.A-9448(A) (PI: Lanzoni), we used KMOS multiple pointings to investigate the region within  $\sim 9''$  and  $70''$  from the center of NGC 6388. The results obtained from these observations are the subject of the present paper, and they prompted us to successfully apply for an ESO Large Program (193.D-0232, PI: Ferraro) aimed at constructing a new generation of VD profiles for a representative sample of Galactic GCs.

In Section 2, we describe the observations and data reduction procedures. Section 3 is devoted to the description of the kinematic analysis, including a number of tests about the performances of KMOS (Section 3.1), the discussion of the determination of the radial velocities of individual stars (Section 3.2), and the presentation of the derived VD profile (Section 3.3). Discussion and conclusions are presented in Section 4.

## 2. OBSERVATIONS AND DATA REDUCTION

KMOS is a second generation spectrograph equipped with 24 IFUs that can be allocated within a  $7.2$  diameter field of view. Each IFU covers a projected area on the sky of about  $2.8 \times 2.8$ , which is sampled by an array of  $14 \times 14$  spatial pixels (hereafter spaxels) with an angular size of  $0.2$  each. The 24 IFUs are managed by three identical spectrographs, each one

handling 8 IFUs (1–8, 9–16, and 17–24, respectively). At the time of the observations discussed here, IFUs 13 and 16 were not usable. KMOS is equipped with four gratings providing a maximum spectral resolution  $R$  between  $\sim 3200$  and  $4200$  over the  $0.8$ – $2.5 \mu\text{m}$  wavelength range. We have used the YJ grating and observed in the  $1.00$ – $1.35 \mu\text{m}$  spectral range at a resolution  $R \approx 3400$ , corresponding to a sampling of about  $1.75 \text{ \AA pixel}^{-1}$ , i.e.,  $\sim 46 \text{ km s}^{-1} \text{ pixel}^{-1}$  at  $1.15 \mu\text{m}$ . This instrumental setup is especially effective at simultaneously measuring a number of reference telluric lines in the spectra of giant stars, for an accurate calibration of the radial velocity, despite the relatively low spectral resolution. An example of the observed spectra is shown in Figure 4, with a zoom around  $1.15 \mu\text{m}$  to show some isolated telluric lines, and around  $1.06$  and  $1.20 \mu\text{m}$  to show some stellar features of interest.

The data presented here have been acquired during the KMOS SV, with four different pointings on NGC 6388. The total on-source integration time for each pointing was 3–5 minutes and it has been obtained with three sub-exposures of 60–100 s each, dithered by  $0.2$  for optimal flat-field correction. The typical signal-to-noise ratio (S/N) of the observed spectra is  $\gtrsim 50$ . We used the “nod to sky” KMOS observing mode and nodded the telescope to an off-set sky field at  $\approx 6'$  north of the cluster center, for a proper background subtraction.

The spectroscopic targets have been selected from near-IR data acquired with SOFI at the ESO-NTT (Valenti et al. 2007), based on the star position in the color–magnitude diagrams (CMD) and the radial distribution within the cluster.

We selected targets with  $J < 14$  mag (in order to always have  $S/N > 50$ ) and sufficiently isolated, without stars brighter than 15 mag within  $1''$  from their center. We then used Advanced Camera for Surveys–*Hubble Space Telescope* data in the *V* and *I* bands, from Lanzoni et al. (2007), Sarajedini et al. (2007), and Dalessandro et al. (2008), to identify additional stars not present in the SOFI catalog.

The raw data have been reduced using the KMOS pipeline version 1.2.6, which performs background subtraction, flat-field correction and wavelength calibration of the two-dimensional (2D) spectra. The one-dimensional (1D) spectra have been extracted manually by visually inspecting each IFU and selecting the spectrum from the brightest spaxel in correspondence with each target star centroid, in order to minimize the effects of possible residual contamination by nearby stars and/or by the unresolved stellar background. An example of the reconstructed images of the stars observed during the first pointing is shown in Figure 1.

We measured a total of 82 giant stars located within  $\sim 70''$  from the center of NGC 6388. Figure 2 shows the position of the targets in the (*I*, *V* – *I*) and (*J*, *J* – *K*) CMDs, while Figure 3 displays their location in the R.A. and decl. plane. Identification number, coordinates, and magnitudes of each target are listed in Table 1 (the complete version of the table is available in electronic form). Twelve stars have been observed twice for cross-checking measurements from different pointings/exposures. Seven stars are in common with the FLAMES-VLT radial velocity sample of L13. In a few cases, within a single KMOS IFU we could extract the spectra of more than one star and measure their radial velocity (see Figure 1).

## 3. KINEMATIC ANALYSIS

To accurately measure the radial velocities of the observed targets, we made use of cross-correlation techniques with

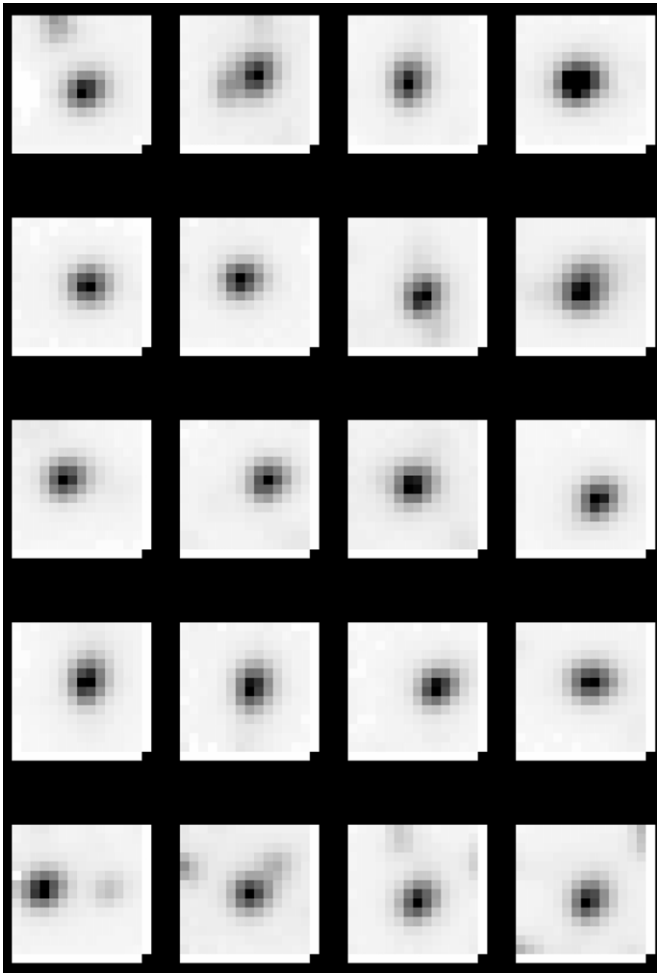


**Figure 1.** Reconstructed images of 20 IFUs obtained during the first pointing. In some cases, other stars with a sufficient spectral S/N and not contaminated by the main target can be recovered from the same IFU.

template spectra (in particular, we used the IRAF task FXCOR). As a telluric template, we used a high-resolution spectrum of the Earth’s telluric features,<sup>5</sup> convolved at the KMOS YJ grating resolution. As stellar templates, we used synthetic spectra

<sup>5</sup> Retrieved from [http://www.eso.org/sci/facilities/paranal/decommissioned/isaac/tools/spectroscopic\\_standards.html](http://www.eso.org/sci/facilities/paranal/decommissioned/isaac/tools/spectroscopic_standards.html).

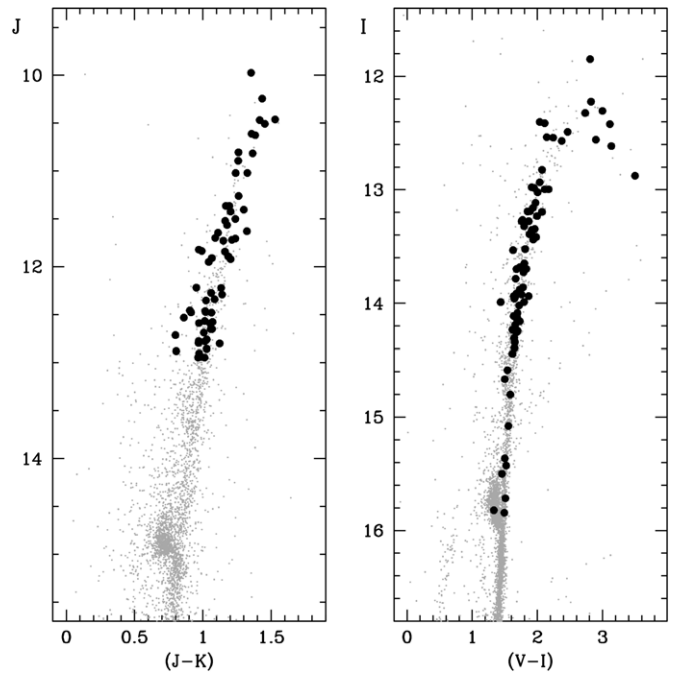


**Figure 2.** ( $J$ ,  $J - K$ ) and ( $I$ ,  $V - I$ ) color–magnitude diagrams (left and right panels, respectively) of NGC 6388, with highlighted the KMOS targets.

computed with the TURBOSPECTRUM code (Alvarez & Plez 1998; Plez 2012), optimized for cool giants. We used a set of average templates with photospheric parameters representative of those of the observed stars and  $[\text{Fe}/\text{H}] = -0.5$  dex, the metallicity of NGC 6388 (see Harris 1996, 2010 edition). For a given star, we also checked the impact of using a different template with varying the temperature by  $\Delta T_{\text{eff}} \pm 500$  K and the gravity by  $\Delta \log g \pm 0.5$  dex and we verified that it has a negligible effect on the final radial velocity measurements ( $< 1 \text{ km s}^{-1}$ ).

### 3.1. Accuracy of the Wavelength Calibration

With the purpose of quantifying the ultimate accuracy of the radial velocity measurements of individual giant stars in crowded fields, we performed a number of tests aimed at checking the reliability and repeatability of the wavelength calibration of each KMOS IFU. Since KMOS is mounted at a Nasmyth focus and rotates, some flexures are expected, with

**Table 1**  
Individual Giant Stars in NGC 6388 Observed with KMOS

Star	R.A. (2000)	Decl. (2000)	$V$	$I$	$J$	$K$	$V_r$	$eV_r$	IFU	Pointing
28786	264.0777424	−44.7539232	15.12	13.32	11.91	10.84	99.7	2.1	18	4
43138	264.0633117	−44.7526742	15.85	14.19	12.90	11.93	75.2	2.4	23	1
43163	264.0631292	−44.7516067	15.64	13.86	12.48	11.42	86.8	4.8	4,19	2,3
78741	264.0976030	−44.7395056	14.94	12.57	10.81	9.54	75.5	1.4	1,11	2,3
81865	264.0950571	−44.7433792	15.94	14.25	12.78	11.81	83.7	6.2	10	3
93646	264.0870297	−44.7361283	15.40	13.42	11.92	10.72	94.1	2.6	6	1
94946	264.0863051	−44.7387495	15.09	13.12	11.57	10.39	83.5	2.8	5	1
96560	264.0849040	−44.7377027	14.52	12.41	10.89	9.63	79.5	1.8	2	2
100296	264.0711060	−44.7360611	15.80	13.94	11.63	10.31	70.5	4.3	3	3
101667	264.0820265	−44.7355902	16.16	14.67	0.00	0.00	84.4	5.2	3	2
.....										

**Note.** Identification number, coordinates, optical and NIR magnitudes, radial velocities ( $V_r$ ), and errors ( $eV_r$ ) in  $\text{km s}^{-1}$ , KMOS IFU and pointing numbers (two values are marked for the 12 targets observed twice).

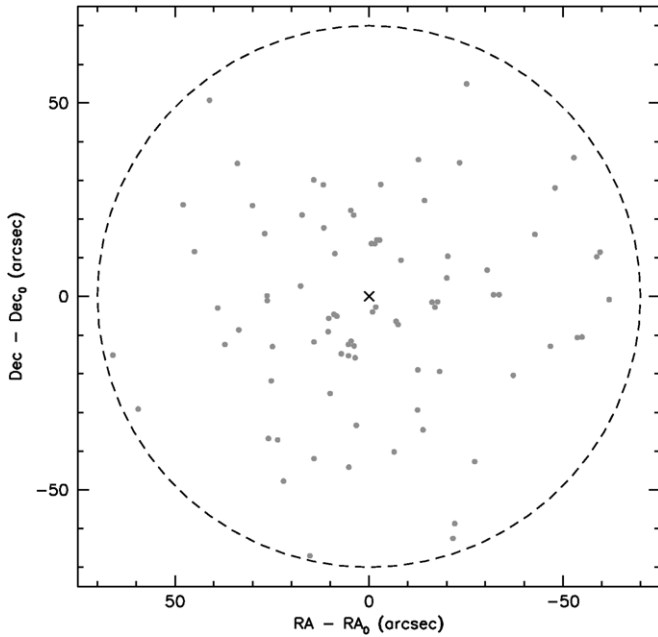


**Figure 3.** Position of the observed target (gray circles) in the central region of NGC 6388. The black cross marks the center of the cluster as derived in Lanzoni et al. (2007) while the black annulus marks a region of  $70''$  of radius.

impact on the overall spatial and especially spectral accuracy of the reconstructed 2D spectra.

The KMOS Data Reduction Software (DRS) pipeline allows us to take calibration exposures at several rotator angles and to

choose the frames with the rotator angle closest to the one of the input science frame and eventually interpolate. The KMOS DRS pipeline also has the option of refining the wavelength solution by means of the observed OH lines. We reduced the spectra by selecting all of these options to obtain the best possible accuracy in the spectral calibration.

However, residual velocity shifts in different spaxels of a given IFU, as well as in different IFUs, are still possible. In order to measure these residual shifts, we selected the spectral region between  $1.14$  and  $1.16 \mu\text{m}$  (see Figure 4) containing telluric lines only, and we cross-correlated the observed spectra from five different spaxels in a given IFU with the telluric template. The five spaxels are the ones where the star centroid is located (having the highest signal) and the four surrounding (cross-shape) spaxels. We then computed the residual wavelength/velocity shifts of the four surrounding spaxels with respect to the central one used as reference. As an example, Figure 5 shows the results for IFU 15: four different stars (245899, 250977, 198027, and 132259) have been observed in four pointings. The measured zero point shifts are normally well within  $\pm 10 \text{ km s}^{-1}$ , corresponding to one-fourth of a pixel at the spectral resolution of the KMOS YJ band,<sup>6</sup> with average values of a few  $\text{km s}^{-1}$  and corresponding dispersions within  $10 \text{ km s}^{-1}$  (see Table 2). For each IFU, we finally combined the spectra from the five spaxels, by using the IRAF task SCOMBINE, and we measured the radial velocity in the resulting combined one. The obtained values (see Figure 5) are fully consistent with the average values from individual spaxels (see Table 2).

<sup>6</sup> At this resolution, one pixel corresponds to  $\sim 46 \text{ km s}^{-1}$ .

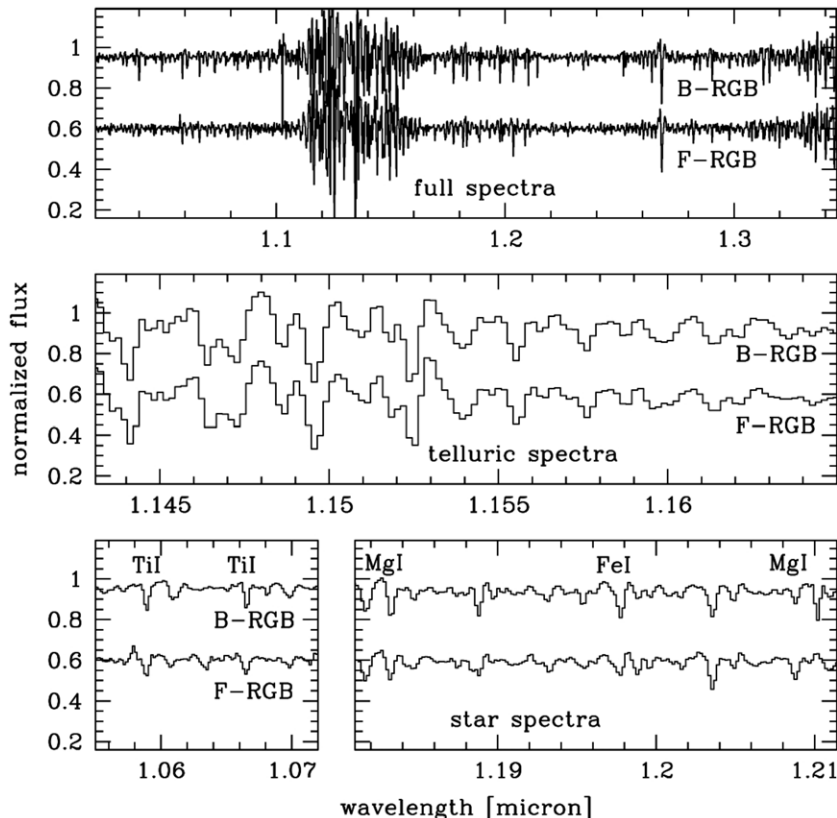


**Figure 4.** Example of the observed KMOS YJ spectra of two giant stars: a bright B-RGB (star 245899,  $J = 10.24$  mag, top spectra) and a faint F-RGB (star 43138,  $J = 12.90$  mag, bottom spectra). Top panel: observed spectra. Middle panel: zoomed spectra around  $1.15 \mu\text{m}$ , including a few isolated telluric lines. Bottom panel: zoomed spectra around  $1.05$  and  $1.2 \mu\text{m}$ , including a few isolated stellar features of interest.

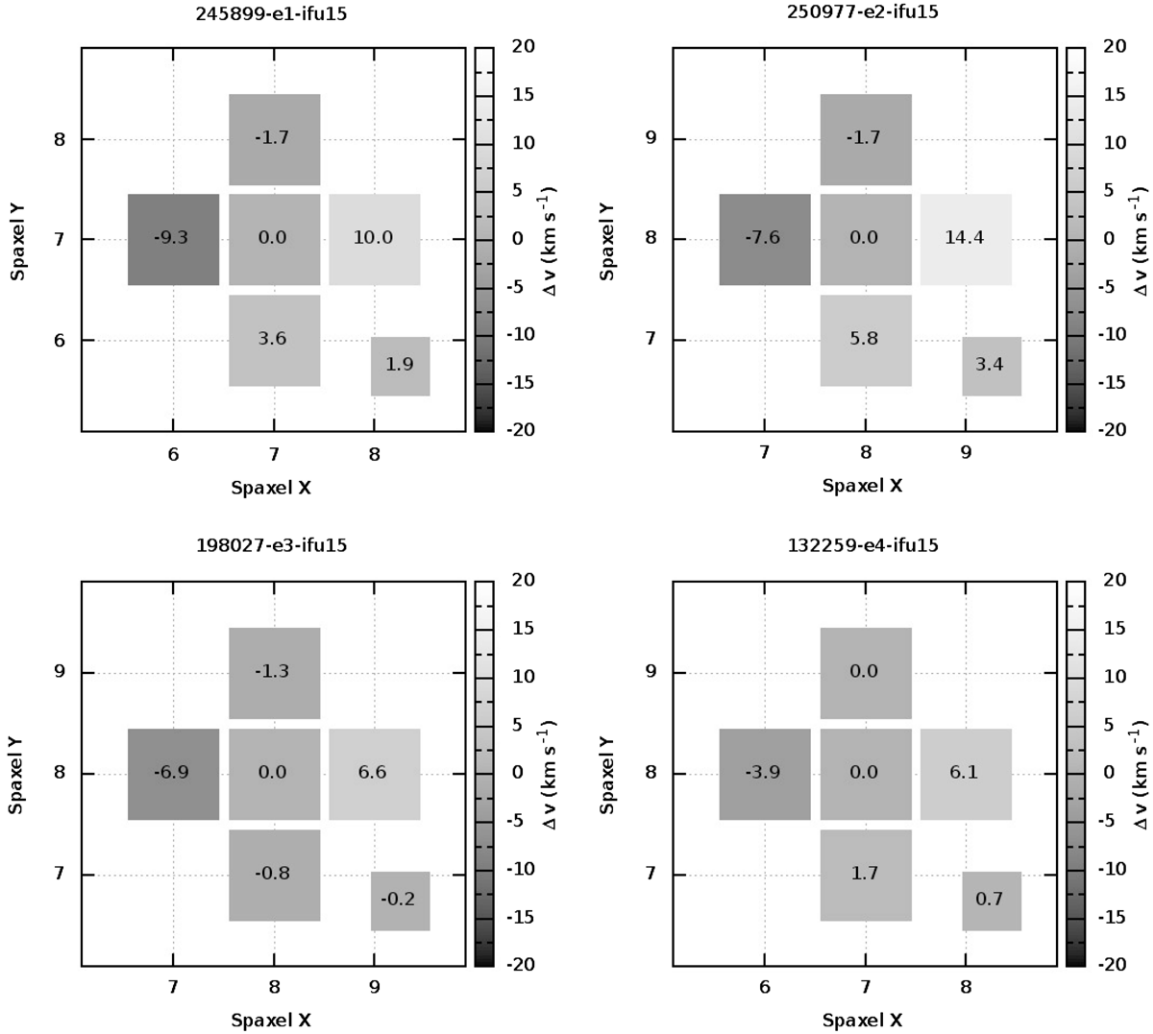


**Figure 5.** Spaxel cross-shaped matrixes used in the wavelength calibration test. The matrixes are centered on the brightest spaxel of stars 245899, 198027, 250977, and 132259 observed with the IFU 15 during pointings 1, 2, 3, and 4, respectively. The number marked in each spaxel refers to the velocity shift (in  $\text{km s}^{-1}$ ) with respect to the central spaxel, as measured by cross-correlating telluric lines. The small square in the bottom-right corner of each matrix marks the velocity shift with respect to the central spaxel, which was obtained directly from cross-correlating the combined (from the five spaxels in the cross) spectrum.

**Table 2**  
Results of the Wavelength Calibration Tests

Star	$\langle \Delta v_{\text{cross}}^{\text{telluric}} \rangle$	$\langle \Delta v_{\text{cross}}^{\text{stellar}} \rangle$	IFU	Pointing
245899	+0.7(8.2)	-1.0(9.2)	15	1
250977	-0.6(5.5)	+2.2(5.7)	15	2
198027	+2.7(9.5)	-0.1(11.8)	15	3
132259	+1.0(4.1)	+0.3(7.1)	15	4
124271	+0.3(8.2)	+0.7(9.7)	20	1
325164	+0.4(8.2)	+1.3(11.5)	11	2
216954	-0.1(5.7)	-0.5(7.8)	2	4

**Notes.** Average velocity shifts and dispersion (in brackets) among different spaxels distributed in cross-shaped matrixes, with respect to the reference central spaxel. Velocity in  $\text{km s}^{-1}$ .

For the same four stars observed with IFU 15, we also used five, isolated stellar lines in two spectral regions centered at 1.06 and 1.20  $\mu\text{m}$  (see Figure 4) to compute the velocity shifts. Also, in this case, for each star we extracted the spectrum of the spaxel with the highest signal and the spectra of the surrounding (cross-shape) spaxels. We cross correlated them with suitable synthetic spectra having photospheric parameters as those of

the target stars. The resulting velocity shifts with respect to the central reference spaxel have been plotted in Figure 6, while the average values are listed in Table 2. The inferred average values and dispersions are fully consistent (at better than one-tenth of a pixel) with those obtained measuring the telluric lines. For each star, we finally combined the spectra from the five spaxels as done in the first test and we measured the radial velocity in the resulting spectra. The obtained values (see Figure 5) are fully consistent with the average values from individual spaxels (see Table 2), as well as with the shifts measured with the telluric lines.

We repeated the same tests by using other stars observed by different IFUs in different pointings. As an example, Table 2 also reports the average shifts for the other three stars, namely 124271, 325164, and 216954 observed by the IFUs 20, 11, and 2 and collected during the pointings 1, 2, and 4, respectively. We found values very similar to those derived for the IFU 15, thus ensuring that the overall wavelength calibration provided by the KMOS DRS pipeline is normally accurate and stable in time at a level of a fraction (on average, within one-tenth) of a pixel, both within each IFU and among different IFUs.

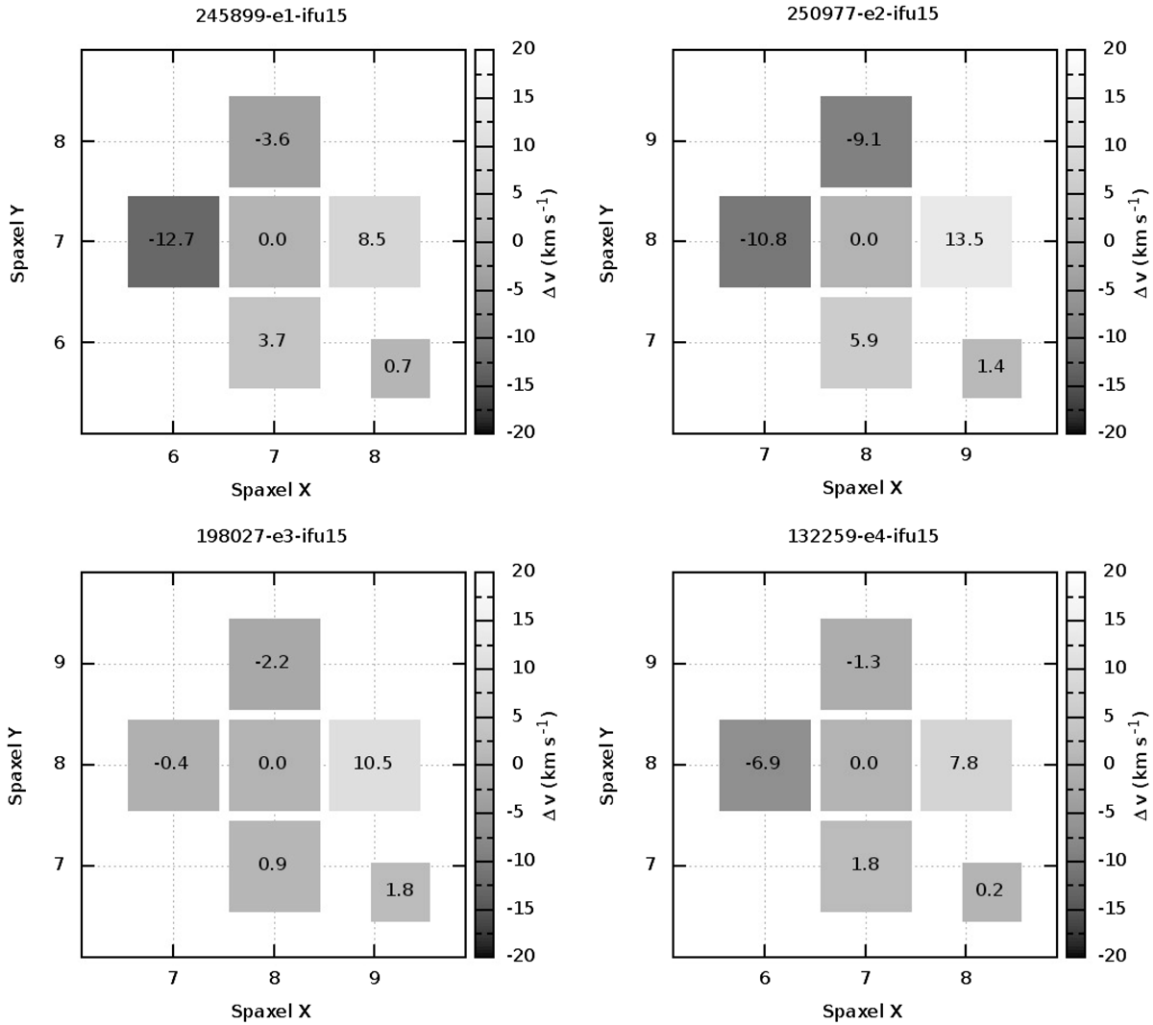


Figure 6. Same as in Figure 5, but for the velocity shifts measured by cross-correlating stellar lines.

The tests performed thus far, by using both telluric and stellar lines, have demonstrated that the velocity shifts between the spectra extracted from the spaxel with the highest signal and those obtained by combining the spectra from the cross-shape spaxels are fully consistent with each other, thus we decided to use the spectra of the brightest spaxel only, which is definitely dominated by the target light. Hence, as a final wavelength calibration check, we selected the spectrum corresponding to the spaxel with the highest signal in each observed star. We then cross-correlated this spectrum with the telluric template as reference, and computed the residual velocity shift. Figure 7 shows the results for the active KMOS IFUs. We find that for a given IFU, the residual velocity shifts as measured in different stars observed during different pointings/exposures are normally consistent to each other with an average dispersion of  $3.4 \text{ km s}^{-1}$ . Such a dispersion is relatively small, taking into account that the four exposures on NGC 6388 were obtained with KMOS at very different rotation angles with respect to the Nasmyth axis ( $261^\circ$ ,  $188^\circ$ ,  $326^\circ$ , and  $97^\circ$  in pointing 1, 2, 3, and 4, respectively), indicating that the KMOS optimized calibration procedure is effective in correcting the effects of spectral flexures.

Since the 24 IFUs of KMOS are managed by three separate spectrographs, one can also compute the mean shift of each spectrograph, by averaging the mean shifts from IFUs 1 to 8, 9

to 16, and 17 to 24, respectively. We find very similar residual velocity shifts, of  $\approx -2 \text{ km s}^{-1}$  and dispersion of  $3\text{--}5 \text{ km s}^{-1}$ .

### 3.2. Radial Velocity Measurements

The tests described in Section 3.1 indicate that the wavelength calibration provided by the KMOS pipeline is well suited for kinematic studies of extragalactic sources. However, for precise radial velocity measurements of individual stars, it is necessary to refine the calibration, by correcting each spectrum for the corresponding residual velocity shift, as inferred from the telluric lines.

Once corrected for such a residual shift, the radial velocity of each star was computed by cross-correlating the observed spectra with suitable synthetic ones. We finally applied the heliocentric correction by using the IRAF task RVCORRECT. The final radial velocity errors have been computed from the dispersion of the velocities derived from each line divided by the number of lines used (that is  $eV_r = \sigma/\sqrt{N_{\text{lines}}}$ ). The average uncertainty in the velocity estimates is  $2.9 \text{ km s}^{-1}$ .

Figure 8 shows the inferred radial velocities as a function of the radial distance from the cluster center and the histogram of their distribution. Table 1 lists the radial velocity values and corresponding errors, as well as the KMOS IFU and pointing reference numbers. For the 12 stars observed twice, the average

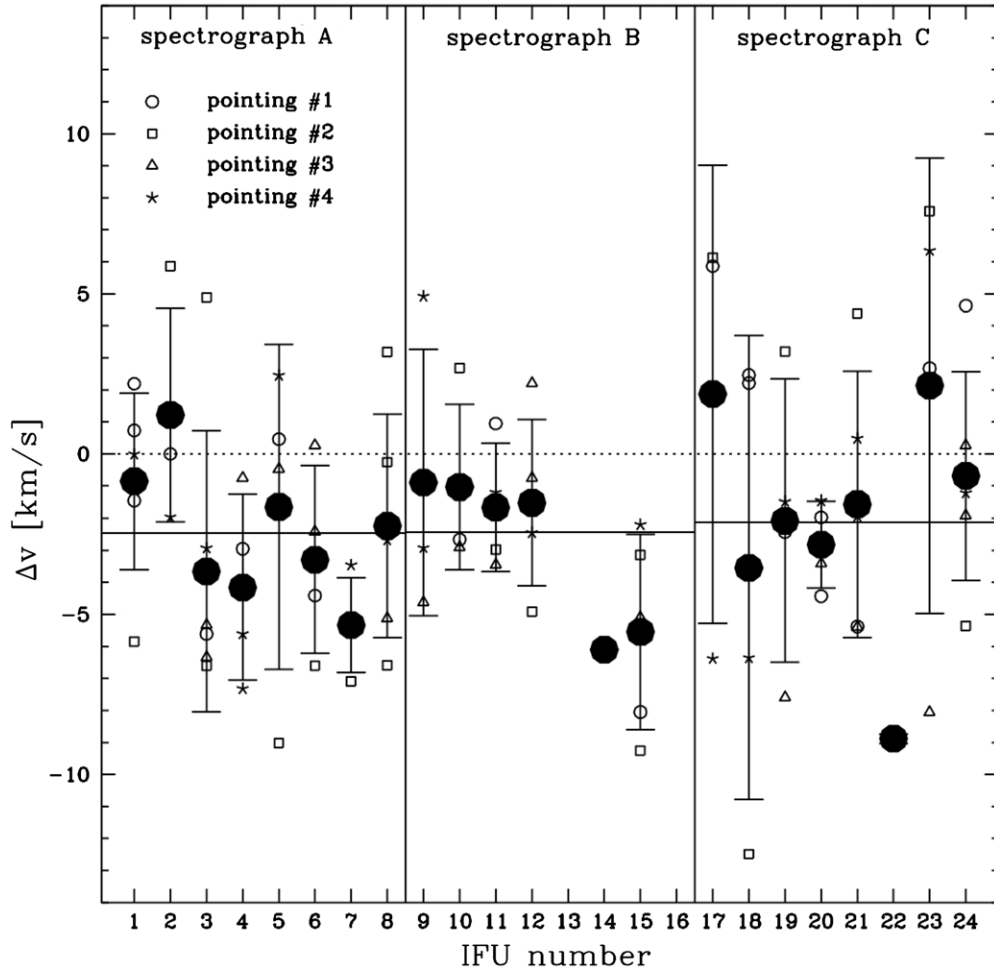


**Figure 7.** Telluric velocity shifts (in units of  $\text{km s}^{-1}$ ) of the spectra extracted from the spaxel with the highest signal for all the target stars observed with the KMOS IFUs (small symbols). The shifts have been computed by using the telluric template as reference. The large dots mark the average values and the  $1\sigma$  dispersion as measured for each IFU, while the horizontal, continuum lines mark the average values for each of the three spectrographs. IFUs 13 and 16 were not usable during those observations.

value of the measured radial velocities has been adopted. For these stars, the measured radial velocities are in excellent agreement, with an average difference of  $\sim 1 \text{ km s}^{-1}$  between two different exposures and a dispersion of  $3.6 \text{ km s}^{-1}$ .

Only seven stars have been found in common with the FLAMES sample of L13, and the inferred radial velocities from the KMOS spectra turned out to be in good agreement with the FLAMES ones. In fact, by applying a  $2\sigma$  rejection criterion, an average difference of  $\langle \Delta V_{\text{KMOS-FLAMES}} \rangle = -0.2 \text{ km s}^{-1}$  ( $\sigma = 2.2 \text{ km s}^{-1}$ ) is found.

We computed the systemic velocity of the KMOS sample by conservatively using all stars with radial velocities between 60 and  $105 \text{ km s}^{-1}$ , as done in L13 for the SINFONI and FLAMES samples. In this velocity range, 75 stars are counted, representing 91% of the entire KMOS sample. We found  $81.3 \pm 1.5 \text{ km s}^{-1}$ , in very good agreement with the value of  $82.0 \pm 0.5 \text{ km s}^{-1}$  found by L13 and indicating that all samples are properly aligned on the same radial velocity scale.

### 3.3. Line-of-sight Rotation and Velocity Dispersion Profiles

To compute the projected rotation and VD profiles from the measured radial velocities of individual stars, we adopted the same approach described in L13. All the 82 KMOS targets have been considered as cluster members, since they all have radial

velocities between 50 and  $130 \text{ km s}^{-1}$ , which has been adopted as cluster membership criterion in L13.

To study the possible presence of a rotation signal, we restricted the analysis to the sample of targets providing a symmetric coverage of the surveyed area, namely 52 stars located between  $9''$  and  $40''$  from the center. To further increase. For further increasing the sample size, we took into account six additional stars in the same radial range from the L13 data set. We then used the method described in Bellazzini et al. (2012, and references therein; see also L13). No significant rotation signal has been found from this sample. Interestingly, however, the distribution of radial velocities for stars within  $20''$  from the cluster center is clearly bimodal (see Figure 8), thus suggesting the possible presence of ordered rotation. Unfortunately, only 23 stars have been measured within this radial range and more data are needed before drawing any firm conclusion about ordered rotation in the central regions of NGC 6388 (see also L13).

To compute the VD profile, we used the entire KMOS sample (but the two innermost targets at  $r < 5''$  have been conservatively excluded) and divided the surveyed area into three radial bins, each containing approximately the same number of stars: namely  $9'' \leq r \leq 23''$  (29 stars),  $23'' \leq r \leq 43''$  (26 stars), and  $43'' \leq r \leq 70''$  (25 stars). The values obtained are  $12.9 \pm 2.0 \text{ km s}^{-1}$ , at an average distance of  $16''$ ,  $12.8 \pm 1.9 \text{ km s}^{-1}$  at  $r = 33''$ , and  $12.2 \pm 1.9 \text{ km s}^{-1}$  at  $r = 56''$ .



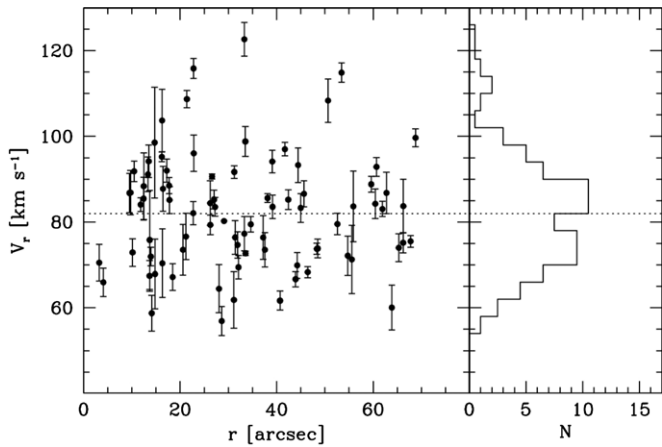


**Figure 8.** Radial velocities as a function of the distance from the cluster center (left panel) and histogram of their distribution (right panel), for the 82 stars of NGC 6388 observed with KMOS. The dotted line marks the systemic velocity of the cluster ( $82 \text{ km s}^{-1}$ ; from L13).

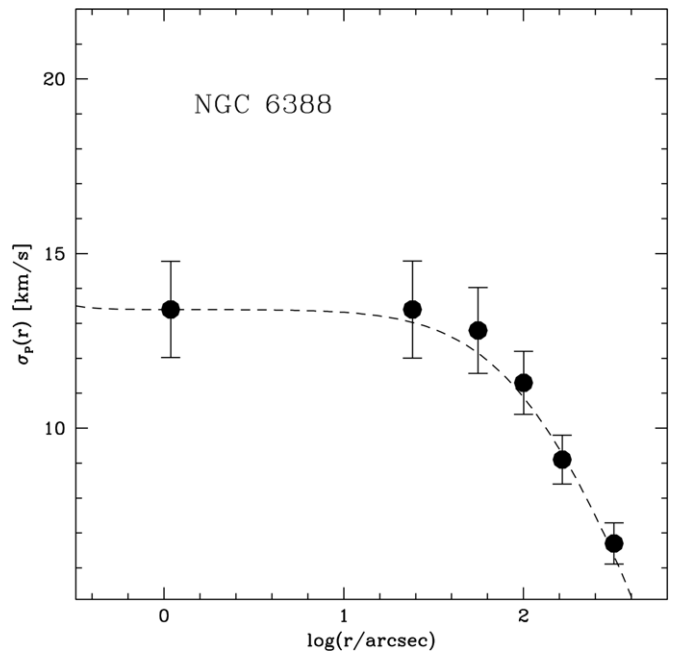


**Figure 10.** Final velocity dispersion profile of NGC 6388, obtained from the combined sample of individual radial velocities, as measured from SINFONI, KMOS, and FLAMES spectra. The dashed line is the same as in Figure 9.

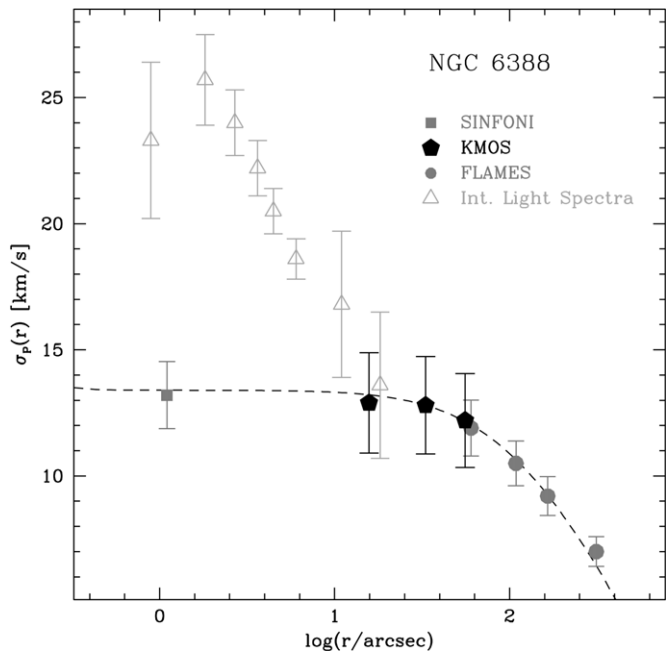


**Figure 9.** Line-of-sight velocity dispersion profile of NGC 6388 computed from the radial velocities of individual stars, as measured with KMOS (black pentagons, this paper), SINFONI, and FLAMES (dark gray squares and circles, respectively; from L13). The dashed line correspond to the self-consistent King model plotted in Figure 13 of L13. The velocity dispersion profile obtained from integrated-light spectra (Lützgendorf et al. 2011) is also shown for comparison (light gray empty triangles).

The errors have been estimated by following Pryor & Meylan (1993). The corresponding profile is plotted in Figure 9.

#### 4. DISCUSSION AND CONCLUSIONS

The VD values obtained with KMOS are presented in Figure 9. We have included for comparison the measurements obtained with SINFONI and FLAMES from L13 and those derived from integrated-light spectra by Lützgendorf et al. (2011). We note that the outermost point of the KMOS VD profile well matches the innermost FLAMES measure of L13. At the same time, the innermost point of the KMOS profile is also consistent with the most external value of Lützgendorf et al. (2011). Overall, the three new KMOS measurements allow us

**Table 3**

Velocity Dispersion Profile of NGC 6388

$r_i$	$r_e$	$r_m$	$N_*$	$\sigma_p$	$e_{\sigma_p}$
0.2	1.9	1.1	51	13.40	1.38
9.0	40.0	24.1	58	13.40	1.39
40.0	75.0	55.9	57	12.80	1.23
75.0	130.0	100.2	81	11.30	0.90
130.0	210.0	164.2	84	9.10	0.70
210.0	609.0	318.8	67	6.70	0.59

**Notes.** The final profile has been obtained from the combined sample of SINFONI, KMOS, and FLAMES spectra. The three first columns give the internal, external, and mean radii (in arcseconds) of each considered radial bin ( $r_m$  is computed as the average distance from the center of all the stars belonging to the bin),  $N_*$  is the number of stars in the bin,  $\sigma_p$  and  $e_{\sigma_p}$  are the velocity dispersion and its rms error (in  $\text{km s}^{-1}$ ), respectively.

to sample the VD profile in the spatial region between  $9''$  and  $70''$ , and better define the knee of the distribution around  $40''$  from the cluster center.

Unfortunately, both crowding and mechanical constraints did not allow us to allocate more than 1–2 KMOS IFUs per pointing in the very central region, i.e., at  $r \leq 9''$ . Hence, given the limited amount of observing time during the SV run, only a few stars have been measured in the innermost region, preventing us to compute a precise VD value closer to the center.

The final VD profile of NGC 6388, obtained from the combination of the entire sample (namely, SINFONI, KMOS, and FLAMES spectra) is presented in Table 3 and shown in Figure 10.

The results presented here demonstrate the effectiveness of an IFU facility to perform multi-object spectroscopy of individual stars even in dense stellar systems and at a modest spectral resolution. The KMOS deployable IFU is especially useful in studying the internal kinematics of GCs for a number of reasons: (1) it allows us to sample stars over a rather large and tunable field of view, according to the cluster central density

and extension; (2) it allows us to measure individual stars and their surroundings, avoiding slit losses and best-accounting for possible blending effects due to crowding and unresolved stellar background; (3) it covers a rather wide spectral range in a single exposure, to simultaneously record stellar features and telluric lines, and measure accurate radial velocities even at a spectral resolution  $R \approx 3000$ .

This research is part of the project Cosmic-Lab (<http://www.cosmic-lab.eu>) funded by the *European Research Council* (under contract ERC-2010-AdG-267675). E.V. acknowledges ESO DGDF (SL) 14/51/E. NSO/Kitt Peak FTS data used here were produced by NSF/NOAO. We warmly thank the anonymous referee for suggestions that improved the paper.

## REFERENCES

- Alvarez, R., & Plez, B. 1998, *A&A*, **330**, 1109  
 Anderson, J., & van der Marel, R. P. 2010, *ApJ*, **710**, 1032  
 Baumgardt, H., Makino, J., & Hut, P. 2005, *ApJ*, **620**, 238  
 Bellazzini, M., Bragaglia, A., Carretta, E., et al. 2012, *A&A*, **538**, A18  
 Binney, J., & Tremaine, S. 1987, in *Galactic Dynamics* (Princeton, NJ: Princeton Univ. Press), 747  
 Dalessandro, E., Lanzoni, B., Ferraro, F. R., et al. 2008, *ApJ*, **677**, 1069  
 Dubath, P., Meylan, G., & Mayor, M. 1997, *A&A*, **324**, 505  
 Einsel, C., & Spurzem, R. 1999, *MNRAS*, **302**, 81  
 Fabricius, M. H., Noyola, E., Rukdee, S., et al. 2014, *ApJL*, **787**, L26  
 Ferraro, F. R., Beccari, G., Dalessandro, E., et al. 2009, *Natur*, **462**, 1028  
 Ferraro, F. R., Lanzoni, B., Dalessandro, E., et al. 2012, *Natur*, **492**, 393  
 Ferraro, F. R., Possenti, A., Sabbi, E., et al. 2003, *ApJ*, **595**, 179  
 Fiestas, J., & Spurzem, R. 2010, *MNRAS*, **405**, 194  
 Harris, W. E. 1996, *AJ*, **112**, 1487  
 Kacharov, N., Bianchini, P., Koch, A., et al. 2014, *A&A*, **567**, A69  
 Kamann, S., Wisotzki, L., & Roth, M. M. 2013, *A&A*, **549**, A71  
 King, I. R. 1966, *AJ*, **71**, 64  
 Lane, R. R., Kiss, L. L., Lewis, G. F., et al. 2010, *MNRAS*, **406**, 2732  
 Lanzoni, B., Dalessandro, E., Ferraro, F. R., et al. 2007, *ApJL*, **668**, L139  
 Lanzoni, B., Mucciarelli, A., Origlia, L., et al. 2013, *ApJ*, **769**, 107 (L13)  
 Lützgendorf, N., Kissler-Patig, M., Gebhardt, K., et al. 2013, *A&A*, **552**, A49  
 Lützgendorf, N., Kissler-Patig, M., Noyola, E., et al. 2011, *A&A*, **533**, A36  
 McLaughlin, D. E., & van der Marel, R. P. 2005, *ApJS*, **161**, 304 (MvM05)  
 McNamara, B. J., Harrison, T. E., Baumgardt, H., & Khalaj, P. 2012, *ApJ*, **745**, 175  
 Meylan, G., & Heggie, D. C. 1997, *A&ARv*, **8**, 1  
 Miocchi, P. 2007, *MNRAS*, **381**, 103  
 Noyola, E., Gebhardt, K., Kissler-Patig, M., et al. 2010, *ApJL*, **719**, L60  
 Plez, B. 2012, *Turbospectrum: Code for Spectral Synthesis*, Astrophysics Source Code Library, record ascl:1205.004  
 Pryor, C., & Meylan, G. 1993, in *ASP Conf. Ser.*, 50, *Structure and Dynamics of Globular Clusters*, ed. S. G. Djorgovski & G. Meylan (San Francisco, CA: ASP), 357  
 Sarajedini, A., Bedin, L. R., Chaboyer, B., et al. 2007, *AJ*, **133**, 1658  
 Sharples, R., Bender, R., Agudo Berbel, A., et al. 2010, *Msngr*, **139**, 24  
 Trenti, M., & van der Marel, R. 2013, *MNRAS*, **435**, 3272  
 Valenti, E., Ferraro, F. R., & Origlia, L. 2007, *AJ*, **133**, 1287  
 Vesperini, E., Varri, A. L., McMillan, S. L. W., & Zepf, S. E. 2014, *MNRAS*, **443**, L79  
 Wilson, C. P. 1975, *AJ*, **80**, 175